Flow analysis on an automotive brake disc with NACA 66-209 airfoils, using particle image Velocimetry

Análisis del caudal en un disco de freno automotriz con álabes de ventilación tipo NACA 66-209, utilizando velocimetría por imágenes de partículas

Ricardo García-León[1]
Jesús Rivera-López[2]
Abner Quintero-Orozco[3]
Guadalupe Gutiérrez-Paredes[4]

[1] Universidad Francisco de Paula Santander, Ocaña (Colombia); Instituto Politécnico Nacional (México); email: ragarcial@ufpso.edu.co

[2] Instituto Politécnico Nacional (México); email: eduardo_rivera@hotmail.com

[3] Universidad Francisco de Paula Santander, Ocaña (Colombia); Instituto Politécnico Nacional (México); email: aquinteroo@ufpso.edu.co

[4] Instituto Politécnico Nacional (México); email: ggutierrez@ipn.mx

Recieved: 06-09-2018 Accepted: 22-02-2019

How to quote: García-León, Ricardo; Rivera-López, Jesús; Quintero-Orozco, Abner; Gutiérrez-Paredes, Guadalupe (2019). Flow analysis on an automotive brake disc with NACA 66-209 airfoils, using particle image Velocimetry. *Informador Técnico, 83(1), 6-18.*
doi: https://doi.org/10.23850/22565035.1785

Abstract

A car's brake system must meet a complex set of important requirements, such as road safety, which is based on the geometric arrangement and type of material. The objective of this work is to propose a new geometric arrangement for the optimization of airflow in an automotive brake disc, taking into account ventilation pillars based on aerodynamic NACA 66-209 profiles. To support this design proposal, additive manufacturing carried out the construction of a 1: 1 scale prototype and the design of an installation that allows the assembly of the disk to measure the speed fields generated in the Suction and discharge zone by Particle Image Velocimetry (PIV). The validation of the geometric arrangement was carried out under five (5) angular speed conditions: 541, 641, 741, 841 and 941 rpm. The results obtained show the optimization of the airspeed in the discharge zone of 0.1151 and 0.2317 m/s at 35 rpm demonstrating the importance of experimental designs with which the geometry of the disc brakes can be improved, self-ventilated and in this way guarantee the efficiency and safety of the system.

Keywords: velocimetry by particle images; brake disc; NACA; speed; geometry; automotive; flow analysis; NACA 66-2019; ventilation blades.

Resumen

El sistema de frenos de un automóvil debe satisfacer un conjunto complejo de requerimientos importantes, tales como la seguridad vial, la cual se basa en función del arreglo geométrico y el tipo de material. El objetivo de este trabajo es proponer un nuevo arreglo geométrico para la optimización del flujo de aire en un disco de freno automotriz, teniendo en cuenta pilares de ventilación fundamentados en perfiles aerodinámicos tipo NACA 66-209. Para sustentar esta propuesta de diseño, se llevó a cabo la construcción de un prototipo a escala 1:1 por medio de manufactura aditiva y al igual que el diseño de una instalación que permite el montaje del disco para medir el campo de velocidades generado en la zona de succión y descarga mediante el uso de la Velocimetría

por Imágenes de Partícula (VIP). La validación del arreglo geométrico se efectuó bajo cinco (5) condiciones de velocidad angular: 541, 641, 741, 841 y 941 rpm. Los resultados obtenidos muestran la optimización de la velocidad del aire en la zona de descarga de 0.1151 y 0.2317 m/s a 35 rpm por evidenciar la importancia de diseños experimentales con los cuales se pueda mejorar la geometría de los frenos de disco, autoventilados y de esta manera garantizar la eficiencia y seguridad del sistema.

Palabras clave: velocimetría por imágenes de partículas; disco de freno; NACA; velocidad; geometría; automotriz; análisis de caudal; NACA 66-2019; álabes de ventilación.

Introduction

The brake system is undoubtedly the most important component for the road safety of the car since it depends on the total or partial detention of the vehicle and, consequently, the integrity of its passengers. Generally, 70 % of the kinetic energy produced in the movement is absorbed by the front disc brake and the remaining 30 % by the rear brake, which is usually drum. During the repetitions in the braking process, the kinetic energy is transformed into thermal energy, due to the friction generated between the braking track and the pad where temperatures of up to 900 °C are reached according to, Talati and Jalallifar (2018), the 90 % of the heat is distributed and absorbed by the disc brake and the remaining 10 % by the pad.

The principle of operation of these systems is based on friction to stop the movement of the vehicle, with the hydraulic pressure that pushes the brake pads against the nodular gray cast iron disc (García-León; Acosta-Pérez; Flórez-Solano, 2015). Because of this phenomenon, considerably high heat is generated during braking due to the absorption of kinetic energy, increasing the friction temperature. This heat dissipates rapidly with the environment (surrounding air) through the convection phenomenon, which is defined as the transfer of heat that occurs between masses at different temperatures (García-León *et al*., 2015). It is important to mention that environmental factors also play an important role in the heat transfer stage to happen. In addition, when the temperature reaches high values, the radiation heat transfer phenomenon occurs, which also helps dissipate energy in the form of heat stored in the disk (García-León *et al*., 2015; Hirasawa; Kawanami; Shirai, 2014; Porta; Echeverría; Aguayo; Cardoso; Stern, 2016).

The maintenance of the disc brakes is cheaper compared to the drum brakes, therefore, the geometric characteristics of the discs depend on the loading and operating capacity, which is an important factor in the initial design phase. In most cases, designs must avoid overheating that arises between the brake and the pad due to the effect of friction, taking into account, also, the physical, mechanical and chemical properties of the materials used in the braking system (Bocîi, 2011; García-León; Pérez-Rojas, 2016). In the design stage of ventilated disc brakes, it is very important to analyze the behavior of the associated thermo-fluids (surrounding air), where the characteristics and operation of the fluids on the surface of the disc can be observed, always guaranteeing the effectiveness of the braking and heat dissipation process by the surface and ventilation channels (Yan; Feng; Yang; Lu, 2015; García-León; Flórez-Solano, 2017; García-León; Flórez-Solano; Acevedo-Peñaloza, 2018).

The heat dissipation heat and the performance of the ventilated disc brakes depend largely on the aerodynamic characteristics of the airflow, through the ventilation channels and the geometry configurations of the disc brake, which are checked using a CAD design software, which includes the Computational Fluid Dynamics (CFD) library (Chi; He; Naterer, 2009; Ho; Athavale; Forry; Hendricks; Steinetz; García-León, 2017).

In an investigation conducted by Jiménez-García *et al*., (2015), a new geometric arrangement for the optimization of airflow in an automotive brake disc is proposed. In this proposal, NACA type ventilation pillars (4418 and 66-219) were used, in order to perform the analysis by particle Velocimetry and, in this way, optimize the suction conditions (Rivera-López; Arciniega-Martínez; Gutiérrez-Paredes, 2018; García-León; Echavez-Díaz; Flórez-Solano, 2018).

Taking into account the above, in the present investigation, we studied the behavior of air particles in an automotive disc brake with NACA 66-209 ventilation pillars by Particle Image Velocimetry (PIV), evaluating the behaviors and conditions of the elements, in order to optimize the systems that incur in any area of engineering (Senatore; Wulfmeier; Vlahinić; Andrade; Iagnemma, 2013; Hu; Tomg; Liu, 2007; Huang; Hwung; Hsiao; Chang, 2010; Echavez-Díaz; Quintero-Orozco, 2017).

Materials and methods

To make a geometric proposal with NACA 66-209 type ventilation channels, the inlet edge must be taken into account, the angle of attack $\beta 1$ can be modified to allow the flow of the maximum air volume necessary to prevent the disc from overheating, as shown in Figure 1, where it started with a value of $\beta 1 = 63^{\circ}$ due to the number of blades that would be part of the disc brake geometry. Likewise, the procedure of the geometric outline of the curvature of a radial centrifugal impeller is presented in general, taking into account the method of the Kaplan error triangle, which considers the total development of the ventilation pillar in its entire length, angles, and thicknesses, in order to establish the mathematical considerations of the surrounding flow in the brake disc. The curvature obtained is used as a guide for the location of the blades inside the ventilated brake disc, as indicated in Figure 2 with a greater number of blades and a value of $\beta 1 = 59.3^{\circ}$ and, in this way, obtain a suitable geometry for this type of brakes.

To carry out a more detailed geometric study on the number of blades that should be placed in the guide curves of the disc, three proposals were made with three different blade densities, because there is no standard on the appropriate number of blades inside a disk. Taking into account the above, numerical experiments were performed with the proposal of three-blade densities of 10, 15 and 20 blades as shown in Figure 3.

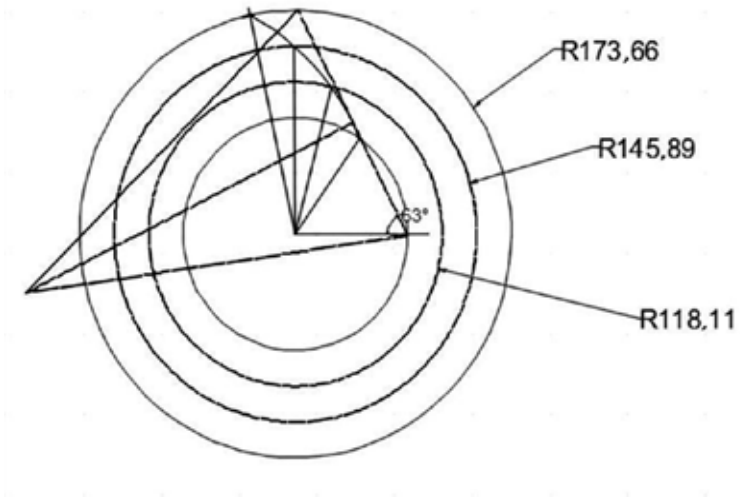

Figure 1. Geometric procedure for the curvature stroke
Source: self made.

Figure 2. Example placement of profiles
Source: self made.

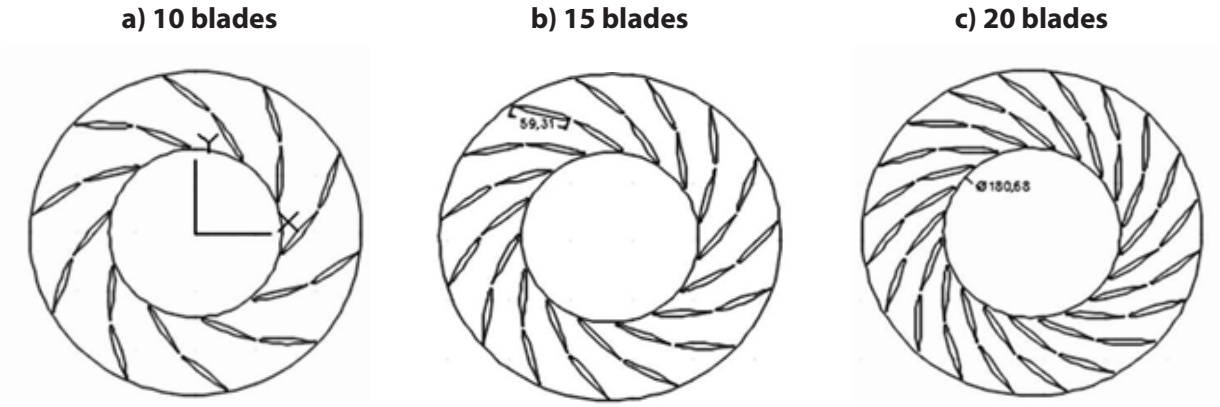

Figure 3. Design for different configurations
a) 10 blades. b) 15 blades. c) 20 blades
Source: self-made.

Tables 1, 2 and 3 were obtained through the ANSYS analysis, which expresses the tangential speed of the airflow circulating through the disk as a function of the angular speed for each number of blades.

Table 1.
Tangential speed (m/s)

No. Blades	541 rpm	641 rpm	741 rpm	841 rpm	941 rpm
10	5.2373	7.2849	8.4055	9.7725	10.7309
15	5.8038	7.2182	9.1452	9.7071	11.6690
20	6.8575	7.3590	9.4147	10.4296	11.3071

Source: self-made.

Table 2.
Pressure change (Pa)

No. Blades	541 rpm	641 rpm	741 rpm	841 rpm	941 rpm
10	93.5014	124.1076	146.1193	175.2459	201.1593
15	95.3727	124.8873	155.0286	177.2354	215.8230
20	110.4992	119.3752	157.0354	185.3101	209.8072

Source: self-made.

Table 3.
Mass flow (kg/s)

No. Blades	541 rpm	641 rpm	741 rpm	841 rpm	941 rpm
10	4.2018	3.6156	4.2018	4.5196	5.2844
15	4.2019	3.5879	4.2019	4.5196	5.2866
20	3.0594	4.3110	4.2019	4.5196	5.2845

Source: self-made.

With the results obtained and the Euler equation for the turbomachines, the term ρ (U_2Vt_2) was calculated, where U_2 is the tangential component of the speed at the exit of the disc tracks and V_{t2} is the absolute velocity of the particle in the same point, the air density is ρ = 1.20 kg/m^3 and the speed U = 2 πNR_D/60, where "N" is the revolutions per minute of the disc and "RD" is the radius of discharge of the brake disc. Likewise, with the results of pressure change ΔP (see Table 2), the aerodynamic efficiency "ψ" was calculated for the three proposed designs, using the following equation 1:

Figure 4 shows the variation of the results as a function of mass flow (see Table 3) and aerodynamic efficiency:

$$\psi = \frac{\rho \ U_2 V_{t2}}{\Delta P} \qquad (1)$$

As seen in Figure 4, aerodynamic efficiency depends on the increases in mass flow, which can be obtained with the following equation 2:

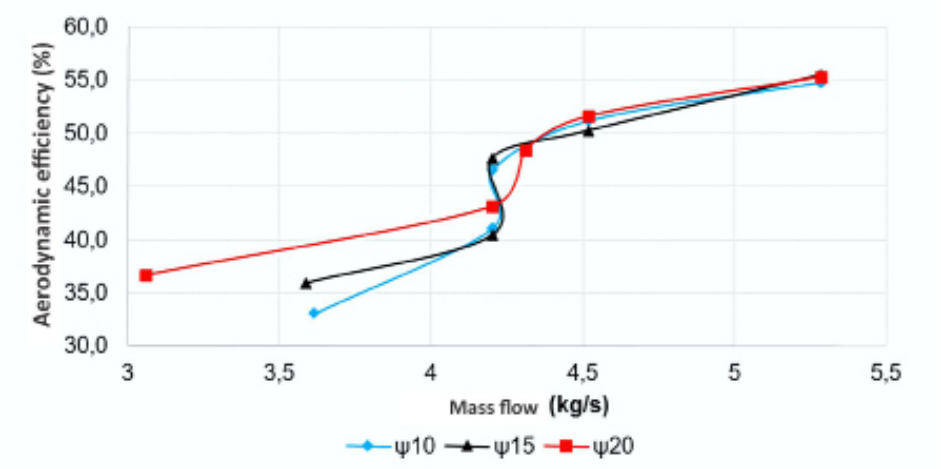

Figure 4. Variation of the aerodynamic efficiency of the three proposed designs
Source: self-made.

On the other hand, since "ψ" is for N = 541 rpm, the blade density equal to 20 has a value of ψ_{20} = 36.66 %, this represents a difference of ψ_{20} - ψ_{15} = 0.74 % and ψ_{20} - ψ_{10} = 3.6 % higher than the other two design proposals.

$$\psi = \psi \ \dot{m} \, (2)$$

However, for this same rotation speed, there is a lower mass flow ($\dot{m}_{20}$ = 3.06 kg/s) compared to densities of 10 ($\dot{m}_{10}$ = 3.61 kg/s) and 15 blades ($\dot{m}_{15}$ = 3.06 kg/s). This way, the existence of blocking or strangulation effects of the visible flow for the disc with 20 blades at low rotation speeds are considered (Rivera-López *et al*., 2018).

Finally, it has concluded that the disc with a density of 15 blades is the best design option, because it has no blocking effects at low speeds and aerodynamics energetically presents a better performance compared to the other two proposals.

Results

An optimal disc braking design with ventilation pillars type NACA 66-209 was selected, where the experimental analysis of Particle Imaging Velocimetry (PIV) was subsequently carried out, carrying out the following activities for the geometric design of the disc Brake:

Disc cutting by laser engraver and cutter

For the manufacture of the disc designed in Solidworks, it was necessary to acquire a 3 mm thick acrylic sheet. Also, the use of a recorder and a laser cutter, where the disc was cut as shown in Figure 5.

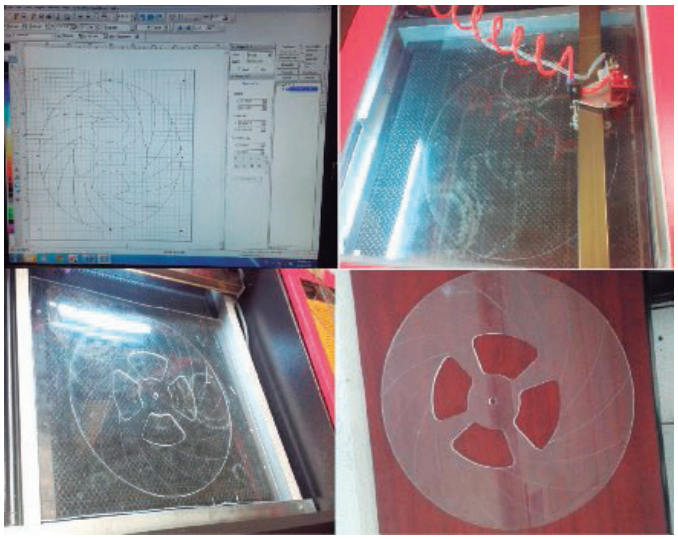

Figure 5. Disc cutting
Source: self-made.

Manufacturing of pillars in 3D printer

After having the base and the disc brake cover for water tests, the NACA 66-209 type ventilation pillars were manufactured, which was made of ABS material, by 3D printing, as shown in the following Figure 6.

Figure 6. Blade Printing
Source: self-made.

Brake disc assembly

After having the base, the cover and the NACA 66-209 ventilation pillars, the components were fixed, which were adjusted with a 3/8 ”threaded shaft as shown in Figure 7 (a). As mentioned earlier, the disc was corrected in order to avoid turbulence in the suction zone, finally remaining as shown in Figure 7 (b).

Figure 7. Assembled disks
a) Assembled disk. b) Assembled Disk Corrected
Source: self-made.

Fluid-dynamic evaluation of the speed field in the suction and discharge of the brake disc by means of PIV (Particle Image Velocimetry)

In this phase, the speed tests for the geometric design of the proposed brake disc were carried out and the images obtained were analyzed. For the analysis we used: 1) a fish tank 1.50 m long, 1.50 m wide and 0.60 m high; 2) a drill where the designed brake disc was adjusted - the revolutions of the drill were controlled by means of a voltage regulator, the revolutions were measured using a tachometer and the drill was adjusted using a wooden support in the center of the fish tank 3) a Red Lake Motion Xtra Model HG-100K fast camera; 4) Motion Central software that was used to visualize the recordings and 5) two 2000 W reflector lamps to give more light to the tests and mustard seeds that represent the particles moving in the water. Taking into account the above, the following experimental procedure was carried out:

Recording with fast camera Red Lake Motion Xtra Model HG-100K. In the configuration of the fast camera, the Motion Central software was used to aim at the blades, have good visibility, adjust the zoom, the resolution, and the necessary focus so that the particles could be clearly visualized. The program setting for recording was established as follows:

Mode: normal
Resolution: 1024x768
Exposition: normal
Section length: 5000
Rank: 60 Frames Per Second (FPS)

Image processing through the Motion Central program and particle tracking in ImageJ. The analysis was performed using water as an operating fluid to facilitate the tracking of particles as they pass through the inside of the disk and thus observe their behavior from entering the suction zone to the exit. For this, it was necessary to make an equivalence between the characteristics of the water and the air because the latter belongs to the real conditions to which the disc is to be operated. The above was done in order to find an equivalence between the speeds of the disk in air and those used in the test of the disk in water assuming that the Reynolds Number for both cases (water and air) must be the same, for what the following equations 3 and 4 were used:

$$Re_{agua} = \frac{V_{agua} * \rho_{agua}}{\mu_{agua}} \qquad (3)$$

$$Re_{aire} = \frac{V_{aire} * \rho_{aire}}{\mu_{aire}} \qquad (4)$$

Where:

Re = Reynolds number
V = Disk rotation speed (rpm)
ρ = Density (kg/m3)
μ = Dynamic viscosity

By equating equations 3 and 4, the variable is cleared V_{water} getting the equation 5:

$$\frac{V_{agua} * \rho_{agua}}{\mu_{agua}} = \frac{V_{aire} * \rho_{aire}}{\mu_{aire}}$$

$$V_{agua} = \frac{(V_{aire})(\rho_{aire})(\mu_{agua})}{(\rho_{agua})(\mu_{aire})}$$

$$V_{agua} = \left(\frac{\rho_{aire}}{\rho_{agua}}\right)\left(\frac{\mu_{agua}}{\mu_{aire}}\right) * V_{aire} \qquad (5)$$

Data for air and water conditions are extracted from Cengel (2007), at an ambient temperature of 22 °C.

$\rho_{aire} = 1.196\ kg/m^3$
$\mu_{aire} = 1{,}82\ x10-5\ Pa/s$
$\rho_{agua} = 997{,}6\ kg/m^3$
$\mu_{agua} = 9.684\ x10-4\ Pa/s$

The values of the speed of rotation of the disc (boundary conditions) are 541, 641, 741 and 841 rpm, equivalent to the linear speeds of the vehicle at 60, 70, 80 and 90 km/h. To calculate the rpm of the disk from the speed of the car, an average value of the wheel radius of 29 cm was assumed, so the conversion factor of km/h to rpm was as follows:

$$1\frac{km}{h}\left(\frac{1000\ m}{1\ km}\right)\left(\frac{1\ h}{60\ min}\right)\left(\frac{1}{0.29\ m}\right)\left(\frac{1\ rev}{2\pi\ rad}\right) = 9.147$$

$$1\frac{km}{h} = \frac{rpm}{9.147}$$

The test for the rpm mentioned above was performed as follows:

$$\frac{541\ \text{rpm}}{9.147} = 59.2 \approx 60 \frac{\text{km}}{\text{h}}$$

$$\frac{641\ \text{rpm}}{9.147} = 70.07 \approx 70\ \frac{\text{km}}{\text{h}}$$

$$\frac{741\ \text{rpm}}{9.147} = 81.01\ \approx 80\ \frac{\text{km}}{\text{h}}$$

$$\frac{841\ \text{rpm}}{9.147} = 91 \approx 90 \frac{\text{km}}{\text{h}}$$

After having the rpm of a disk in an air test, the speeds for the water test were calculated and in this way the equivalence between data was obtained, using equation 5:

$$V_{agua} = 0{,}064 * V_{aire}$$

$$V_{agua} = 0{,}064 * 541 = 35\ \text{rpm}$$

$$V_{agua} = 0{,}064 * 641 = 41\ \text{rpm}$$

$$V_{agua} = 0{,}064 * 741 = 48\ \text{rpm}$$

$$V_{agua} = 0{,}064 * 841 = 54\ \text{rpm}$$

The speeds for the water test equivalent to the air test are 35, 41, 48 and 54 rpm, respectively. For greater relevance of the data, the test was performed in two ways. In the first, the particles (mustard seeds) were deposited in the disc suction zone and after that, the drill movement began. This movement was described as "submerged." The second way was to first operate the drill to start the rotary movement and after a few seconds, the particles were thrown. This movement was called "in rotation".

Figure 8 details the tracking of a particle and its total trajectory while crossing the blade zone for each speed described above.

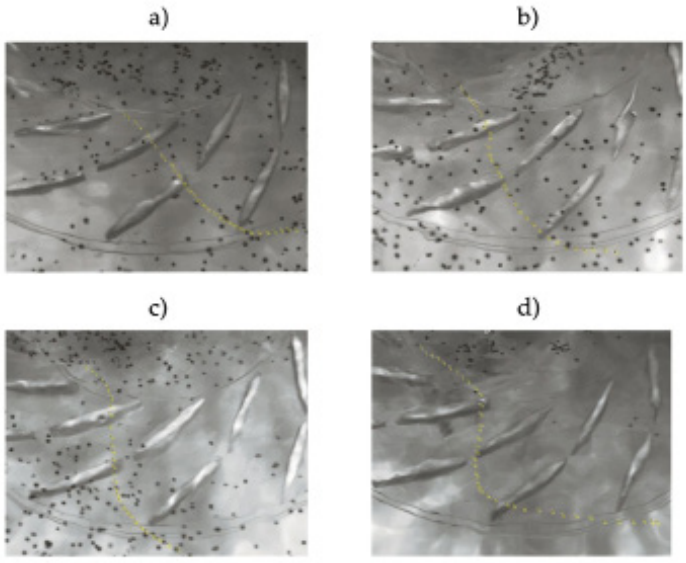

Figure 8. Path of the particles at different speeds
a) Total trajectory 35 rpm in rotation. b) Total trajectory 41 rpm in rotation
c) Total trajectory 48 rpm in rotation. d) Total trajectory 48 rpm in rotation
Source: self-made.

The previous figure shows the general movement of the particle as it passes through the inside of the disc's tracks. Each point shown in the previous sequence of images is represented in this image so that the general behavior can be appreciated. It should be noted that the more vertical the movement, the greater the speed of the particle.

Analysis of results

After processing the images in ImageJ, the values of the coordinates of each particle along its path through the brake disc were obtained. The coordinates were given by the software in pixels and subsequently converted to millimeters. The conversion is obtained from the measurement of a blade in pixels and its actual measurement and, in this way, the conversion factor is reached. The measurement of the blade in pixels is 381,2151623 px and in millimeters, it is 59.24. These values give us a ratio of 0.155397806 mm for each pixel. Having the particle positions in millimeters, its speed was determined by calculating the displacement and time elapsed between each image, from which Figures 9, 10 11, and 12 were obtained):

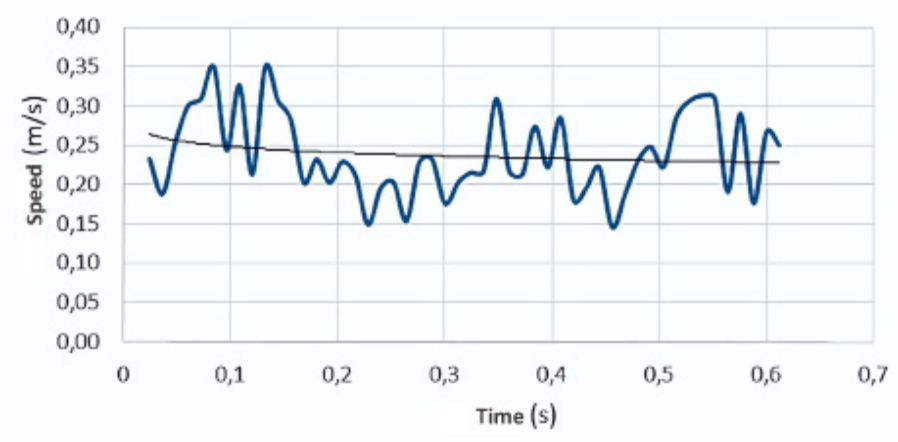

Figure 9. The radial speed at 35 rpm in rotation
Source: self-made.

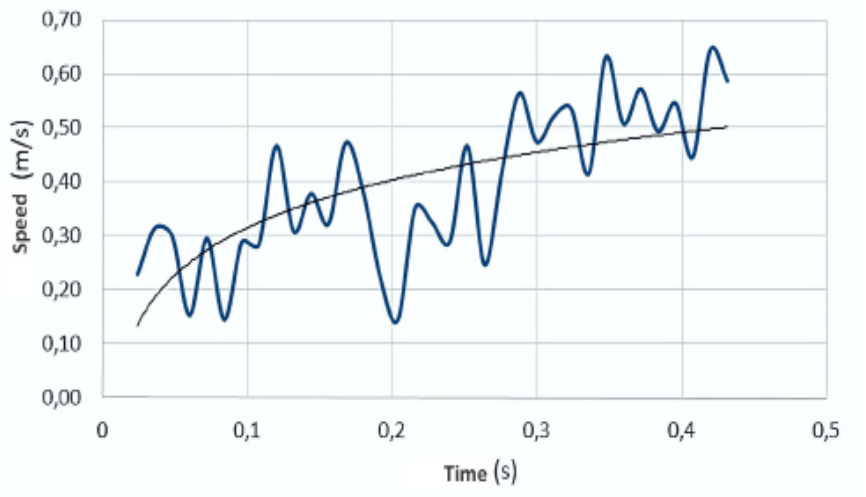

Figure 10. The radial speed at 41 rpm in rotation
Source: self-made.

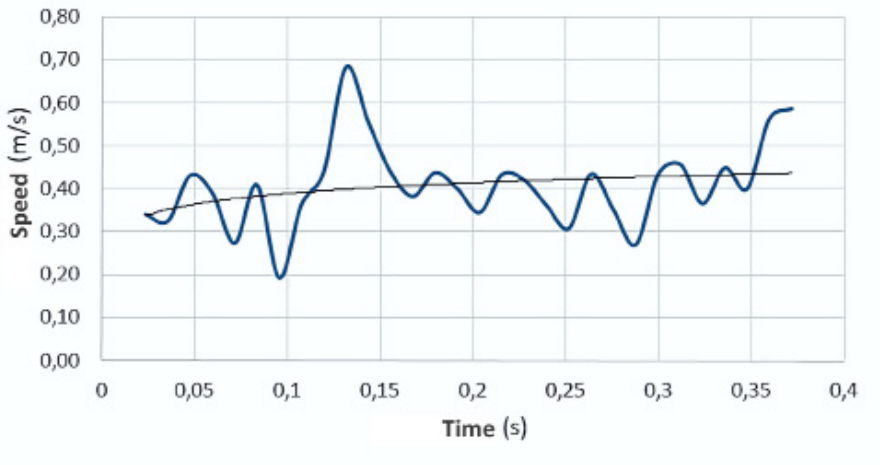

Figure 11. The radial speed at 48 rpm in rotation
Source: self-made.

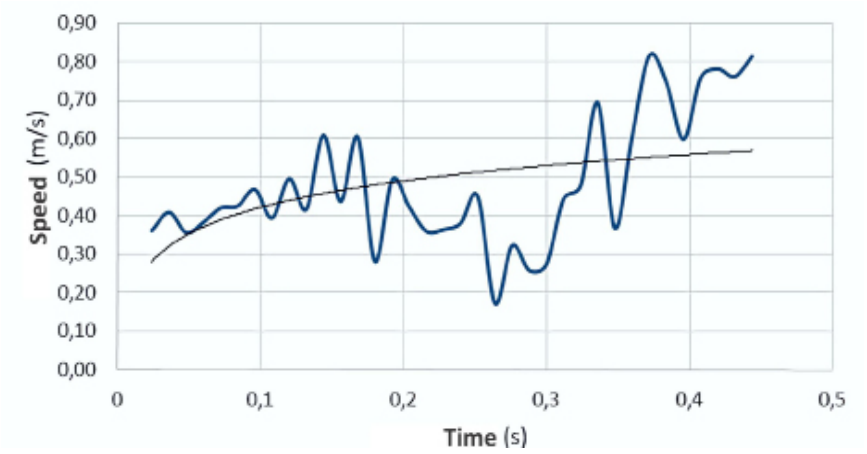

Figure 12. The radial speed at 54 rpm in rotation
Source: self-made.

The previous figures show the behavior of the particles along their route through the ventilation channels in the disc brake, so it can be assumed as the speed of the brake increases, the suction of the air particles increases and, therefore, disk cooling will be much faster in terms of heat transfer and aerodynamics.

Conclusions

The initial speed for each submerged and rotating test shows a difference between each rpm, respectively. In the case of 35 rpm equivalent to a car going at a speed of 60 km/h, in the submerged test it starts with a speed of 0.1151 m/s and for the rotating test, the particle starts with a speed of 0.2317 m/s in the first section, speed that remains constant during the course of the test; while for the first case, the speed carries an ascending sequence. This is because in the test with the submerged particles before starting the movement, the disc starts with a speed of 0 rpm, there is no suction force and, therefore, the particles are at rest, and in the test with the rotating disk, when the particles are thrown, they are instantly attracted to the suction zone of the disk caused by the previous rotating movement.

As the speed of the car increases, the suction is greater, so the test time is generally shorter for each test at a higher speed. This accelerated flow compensates the amount of heat produced at the time of braking because there is a greater amount of energy to reduce the vehicle.

Finally, for the configuration of 20 blades the blockage in the airflow was evidenced at low rotation speeds (N = 541 rpm), this due in large part to the reduction of the effective surface area of the brake disc, that is to say, the amount of blades directly impairs the air circulation. Having the above in mind, it is concluded that the disc with the blade configuration of 15 is the best design option since it has no blocking effects at low speeds and its optimal performance in operation.

References

Bocîi, L. S. (2011). The influence of braking time on heat flow through the friction surfaces of the friction elements of disk brakes for railway vehicles. *Transport, 26(1)*, 75–78. https://doi.org/10.3846/16484142.2011.563494

Cengel, Y. (2007). *Transferencia de calor y masa. Un enfoque práctico.* (3ra ed). México: McGraw-Hil.

Chi, Z.; He, Y.; Naterer, G. (2009). Convective heat transfer optimization of automotive brake discs. *SAE International Journal of Passenger Cars - Mechanical Systems*, 2(1), 961–969. https://doi.org/10.4271/2009-01-0859

Echavez-Díaz, R. D.; Quintero-Orozco, A. (2017). *Estudio experimental del comportamiento dinámico del fluido del aire a través de un disco de freno automotriz con pilares de ventilación tipo NACA 66-209* (tesis de pregrado). Universidad Francisco de Paula Santander, Ocaña, Santander.

García-León, R. A. (2017). Thermal study in three vented brake discs, using the finite element analysis. *DYNA*, 84(200), 19–27. http://dx.doi.org/10.15446/dyna.v84n200.55663

García-León, R. A.; Acosta Pérez, M. A.; Flórez-Solano, E. (2015). Análisis del comportamiento de los frenos de disco de los vehículos a partir de la aceleración del proceso de corrosión. T*ecnura, 19* (45), 53–63. https://doi.org/10.14483/udistrital.jour.tecnura.2015.3.a04

García-León, R. A.; Echavez-Díaz, R. D.; Flórez-Solano, E. (2018). Análisis termodinámico de un disco de freno automotriz con pilares de ventilación tipo NACA 66-209. *INGECUC, 14* (2), 9–18. https://doi.org/10.17981/ingecuc.14.2.2018.01

García-León, R. A.; Flórez-Solano, E. (2017). Dynamic analysis of three autoventilated disc brakes Análisis dinámico de tres frenos de disco autoventilados. *Ingeniería e Investigación*, 37(3), 102–114. https://doi.org/10.15446/ing.investig.v37n3.63381

García-León, R. A.; Flórez-Solano, E.; Acevedo-Peñaloza, C. (2018). *Análisis termodinámico en frenos de disco.* Bogotá, Colombia: ECOE Ediciones.

García-León, R. A.; Pérez-Rojas, E. (2016). Analysis of the amount of heat flow between cooling channels in three vented brake discs. Ingenieria y Universidad, 21(1), 71-96. https://doi.org/10.11144/Javeriana.iyu21-1.aahf

Hirasawa, S.; Kawanami, T.; Shirai, K. (2014). Numerical analysis of convection heat transfer on high-temperature rotating disk at the bottom surface of the airflow duct. In *ASME International Mechanical Engineering Congress and Exposition, Proceedings (IMECE)* (Vol. 8A). Dept. of Mech. Engineering, Kobe University, 1-1 Rokkodai, Nada-Kobe, Hyogo, Japan.
https://doi.org/10.1115/IMECE2014-36142

Ho, Y.-H.; Athavale, M. M.; Forry, J. M.; Hendricks, R. C.; Steinetz, B. M. (1996). Numerical simulation of secondary flow in gas turbine disc cavities, including conjugate heat transfer. In *ASME 1996 International Gas Turbine and Aeroengine Congress and Exhibition, GT 1996* (Vol. 1). CFD Research Corporation, Huntsville, AL, United States.
https://doi.org/10.1115/96-GT-067

Hu, W.; Tomg, B.; Liu, H. (2007). Dynamics of free straight swimming of angulla angulla including forward, braking and backward locomotion. *Journal of Hydrodynamics, Ser. B, 19* (4), 395–402.
http://dx.doi.org/10.1016/S1001-6058(07)60132-2

Huang, Z. C.; Hwung, H. H.; Hsiao, S. C.; Chang, K. A. (2010). Laboratory observation of boundary layer flow under spilling breakers in surf zone using particle image velocimetry. *Coastal Engineering, 57*(3), 343–357.
http://dx.doi.org/10.1016/j.coastaleng.2009.11.004

Jiménez-Garcia, C. A.; Rivera-López, J. E.; Casillas-Navarrete, J. M.; Gutiérrez-Paredes, G. J.; Medina-Ovando, A.; Arciniega-Martínez, J. L. (2015). Medición del campo de velocidad en la succión y descarga de un disco de freno automotriz con pilares de ventilación tipo gota, por medio de Velocimetría por Imágenes de Partículas (PIV). *Revista Congreso Iberoamericano de Ingeniería Mecánica,* (1), 1–9.

Porta, D.; Echeverría, C.; Aguayo, A.; Cardoso, J. E. H.; Stern, C. (2016). Measurement of the Density Inside a Supersonic Jet Using the Background Oriented Schlieren (BOS) Technique. En J. Klapp., L. Di G Sigalotti., A. Medina., A. López., A. Ruiz-Chavarría (Ed.). *Recent Advances in Fluid Dynamics with Environmental Applications.* (115-124). Suiza: Springer Link.
https://doi.org/10.1007/978-3-319-27965-7

Rivera, J.; Arciniega, J.; Gutiérrez, G. (2018). Estudio numérico del comportamiento dinámico del flujo de aire a través de un disco de freno automotriz con pilares NACA 66-209. *REMAI, Revista Multidisciplinaria de Avances de Investigación, 4*(1), 13-22.

Senatore, C.; Wulfmeier, M.; Vlahinić, I.; Andrade, J.; Iagnemma, K. (2013). Design and implementation of a particle image velocimetry method for analysis of running gear–soil interaction. *Journal of Terramechanics, 50*(5), 311–326.
http://dx.doi.org/10.1016/j.jterra.2013.09.004

Talati, F.; Jalallifar, S. (2018). Investigation of heat transfer phenomena in a Ventilated Disk Brake Rotor with Straight radial rounded vanes. *Applied Sciences, 20* (8)(1812-5654), 3583–3592.

Yan, H. B.; Feng, S. S.; Yang, X. H.; Lu, T. J. (2015). Role of cross-drilled holes in enhanced cooling of ventilated b*rake discs. Applied Thermal Engineering, 91*, 318–333.
https://doi.org/10.1016/j.applthermaleng.2015.08.042